Hindawi
Advances in Civil Engineering
Volume 2020, Article ID 4125428, 14 pages
https://doi.org/10.1155/2020/4125428

Research Article

An Innovative Method for Conventional Triaxial Tests of Concrete: Applications of PVC Pipes as a Mould and Sealing Membrane

Zhe Wang,[1] **Xiaoguang Zhou**,[1] **and Jili Feng**[2]

[1]*School of Civil Engineering, Beijing Jiaotong University, Beijing 100044, China*
[2]*State Key Laboratory for Geomechanics and Deep Underground Engineering, China University of Mining and Technology Beijing, Beijing 100083, China*

Correspondence should be addressed to Zhe Wang; zhwang@bjtu.edu.cn

Received 11 January 2020; Revised 24 April 2020; Accepted 2 May 2020; Published 25 August 2020

Academic Editor: Yann Malecot

In this paper, we propose an innovative method for conventional triaxial tests of concrete with a confining cell. The polyvinyl chloride (PVC) pipe is used as a mould to cast concrete and also as a membrane to isolate the concrete specimen from oil under confinements. This method is termed as PMM (i.e., PVC pipe is used as a mould and membrane). However, a heat-shrink sleeve is used as a membrane in the traditional test method (TMM). Specimens were made from mortar without coarse aggregates in the present experiment. Under six confinements (0–70 MPa), the conventional triaxial compression tests were performed on ultrahigh-strength (150 MPa) and high-strength (82 MPa) mortar specimens by PMM and TMM. The results indicate the following: (i) there is a characteristic confinement p_0; when the confinement is lower than p_0, the strength by PMM is higher than that by TMM; on the contrary, when the confinement is higher than p_0, the strengths by both methods are almost identical. In this work, p_0 is between 0 and 5 MPa. (ii) When the confinement is 5–70 MPa, the relationship between the peak stress of high-strength mortar and confinement is characterized by a monotonically rising straight line; however, a monotonically rising upward convex curve describes the peak stress of ultrahigh-strength mortar related to the confinement. (iii) The residual strength using PMM is significantly higher than that using TMM at zero confinement or lower confinements, but the residual strengths by these two methods are approximately identical at higher confinements. (iv) The transverse cracks appear in the mortar specimen inside the PVC pipe after enduring a triaxial loading using PMM. However, there is no such phenomenon when TMM is applied.

1. Introduction

Cylindrical specimens are usually used in conventional triaxial tests of concrete, which can be prepared by drilling cores [1, 2] or casting in concrete moulds [3, 4]. The liquid is used as a medium in conventional triaxial testing machines to apply confinement, and membranes are employed to seal specimens. The membrane materials cover polymers and thin metals with good deformability (such as copper [5]). The commonly used polymer materials include latex, nitrile, silicone, neoprene, and other flexible materials [6–10]. Most testing machines apply oil pressure to confine a specimen. Generally, the range of oil pressure is suitable for almost all confinements from high to low. Wang et al. [8] sealed the specimen with a heat-shrink sleeve. Malecot et al. [9] used a multilayer membrane composed of 8 mm of latex and 2 mm of neoprene under a very high confinement of 650 MPa. For some tests with special requirements, water is taken as a medium, and the confinement is generally below 10 MPa. Chen et al. [10] used a rubber membrane of 2 mm and another latex membrane of 0.4 mm to seal the specimen together. Bjerkeli et al. [11] coated epoxy on the specimen surface for sealing.

The experimental results have indicated that the membrane influences the uniaxial strength of a specimen. For example, Li and Ansari [12] examined the confining effect of the rubber membrane on axial stresses by comparing the uniaxial compressive strengths of jacketed and bare specimens. It showed that the rubber membrane resulted in a 7%

increase in axial strength. However, Sovják et al. [13] demonstrated that the membrane they used did not influence the uniaxial compressive strength. Therefore, different membranes have different impacts on concrete strength.

The membrane is deformed under the action of confinement [14–16]. When a clip gauge was used to measure the radial deformation of the specimen, Candappa et al. [14] passed ten metal studs through the membrane to avoid erroneously including the membrane deformation in measurement results. One end of the stud was in direct contact with the concrete surface, and the other end was connected through a piano wire to the two measuring arms of the clip gauge. The gap between the metal stud and the membrane was filled with a sealant to prevent the oil from penetrating. Lu and Hsu [15] used the same loading scheme to perform two separate triaxial tests on a specimen-size solid steel rod, with and without the membrane, respectively. The radial strains under different confinements were measured, and the difference between them was the decrease in membrane thickness under confinements. In calculating the actual deformation of the specimen, the thickness change of the membrane should be subtracted from the total deformation. When the gauge glued on the specimen surface was used to measure the deformation, the specimen and the gauge should be sealed together by the membrane. If there are pores on or near the specimen surface, the flexible membrane is likely to crush the gauge or its wire on pores under the action of the confinement. Gabet et al. [17] used a PVC shield which is locally set up on gauges as an additional protection. The PVC shield acts as a plane support surface to keep gauges from being pressed into pores.

PVC pipes have extensive applications in the construction industry [18], and their compression performances under axial loads [19] have been studied. Concrete with the PVC pipe refers to a structural member where the PVC pipe and the concrete inside it bear loads together. However, there are few reports on its research. Kurt [20] studied the effect of the slenderness ratio on the strength of concrete with the PVC pipe. The experimental results in [21] showed that both concrete strength and PVC pipe thickness have significant effects on the compressive strength of concrete with the PVC pipe, and a similar observation was reported by Saadoon [22]. These experiments show that the concrete with the PVC pipe outperforms the concrete without the PVC pipe in strength and ductility.

This paper proposed an innovative type of conventional triaxial test method (PMM). We use the PVC pipe as a mould to cast concrete and as a membrane to isolate oil during the testing. Compared with the traditional test method (TMM), PMM has the following advantages:

(1) In the process of concrete forming, PVC pipes as disposable moulds are suitable for casting a large number of concrete specimens at one time. Currently, PVC pipes are priced relatively low and in ample supply in various diameters. They can be used to form concrete specimens with various diameters and heights. In addition, PMM is free from cleaning, assembling, and disassembling moulds, which is a huge boost to test efficiency.

(2) In the process of specimen processing, PMM is more convenient for specimen cutting and grinding, see Section 2.2 for details.

(3) In the process of triaxial loading, the PVC pipe can also be used to isolate the oil from the concrete, thereby simplifying the specimen sealing process before the triaxial test (refer to Section 2.3 for details).

If coarse aggregates are used in concrete, it is worth noting that PMM also has an edge effect like TMM.

2. Materials and Experiments

2.1. Materials and Specimens. In the test, the cement applied was P·II52.5R type Portland cement according to the Chinese standard. The average diameter of the silica fume ranged from 0.1 to 0.3 μm. The average diameter of the quartz powder was 75 μm. Two types of quartz sands in the diameter range 180–425 μm and 425–800 μm, respectively, were mixed by the mass proportion of 1 : 1, and they were used as fine aggregates. The silica fume and the quartz powder were used at the replacement percentages of 20% and 27% for the cement to fill up voids that exist in ultrahigh-strength mortar as well as to improve mechanical properties. The cellulose ether (CE) used in low-strength mortar could prevent mortar from bleeding. We proportionally used the polycarboxylate superplasticizer admixture (PSA) and the liquid defoamer (LD). The PVC pipes have a nominal pressure of at least 1 MPa and are 50 mm in diameter and 2.4 mm in thickness. The mechanical properties of the PVC pipe are presented in Section 3. The mix proportions are given in Table 1. Given the small size of the specimen, no coarse aggregate was used in the specimen.

The mixed mortar was poured into several PVC pipes, each of which is 135 mm in height, and is sealed at the lower end by the tape. The specimens were then vibrated on a shaking table to remove the entrapped air bubbles. Before the specimens were kept in the standard curing room for four days, they were covered with a plastic film. The specimens were then cured for six days in a high-temperature curing box at 90°C. Afterward, the specimens were taken out and cured atmospherically for 90 days regardless of the aging effect on mortar strength. Meanwhile, three kinds of cubic mortar specimens with a side length of 70.7 mm were prepared, and their average uniaxial compressive strengths for 100 days are listed in Table 1. The standard deviation for average uniaxial compressive strength of each mortar is also listed in Table 1.

2.2. Specimen Processing. In the course of cutting, the corner of the mortar specimen surrounded by nothing is often damaged (see Figure 1(a)) due to the diagonal pulling effect of the cutter blade. For the specimen surrounded by the PVC pipe, however, the radial restraint provided by the PVC pipe can weaken the diagonal tension generated by the cutter blade, thus it can prevent damage on the mortar corner. As can be seen from Figure 1(b), there is no damage when the specimen is surrounded by the PVC pipe.

Table 1: Mix proportions and cube compressive strength.

Mortar type	Cementitious material (kg/m^3)		Quartz powder (kg/m^3)	Quartz sand (kg/m^3)	Admixture (kg/m^3)			Water (kg/m^3)	Strength (MPa)	Standard deviation (MPa)
	Cement	Silica fume			PSA	LD	CE			
Low strength	680.0	0	0	884.0	0	0	1.360	353.6	17	0.5
High strength	832.0	0	0	1081.6	0	0	0	316.2	82	2.6
Ultrahigh strength	837.0	167.4	226.0	837.0	30.132	3.013	0	200.9	150	5.1

Notes. PSA: polycarboxylate superplasticizer admixture; LD: liquid defoamer; CE: cellulose ether.

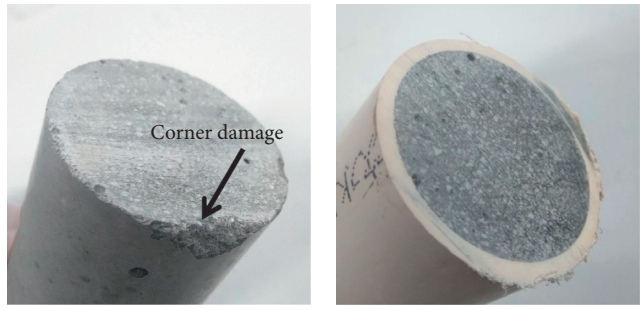

(a) (b)

Figure 1: (a) Mortar surrounded by nothing. (b) Mortar surrounded by the PVC pipe.

In the process of grinding, we find that the mortar specimens surrounded by the PVC pipe are easier to grind into a plane meeting the flatness requirements than those surrounded by nothing. Therefore, it is recommended that the mortar specimen should be surrounded by the PVC pipe during cutting and grinding.

The processed specimens are categorized into two types, i.e., P Specimen (PS) which is the mortar specimen surrounded by the PVC pipe and T Specimen (TS) which is the PS removed from the PVC pipe. The outer and inner diameters of the PVC pipe are 50 mm and 45.2 mm, respectively. The heights of PS and TS are 120 ± 1 mm, and the angle between the normal direction of the specimen end face and the axis of the specimen is not more than 0.25°.

2.3. Specimen Sealing. The specimen is placed between the upper and lower loading heads and is directly contacted with both. The upper loading head is 50 mm in diameter, with a spherical joint; the lower loading head is 53 mm in diameter, slightly larger than the diameter of the specimen.

To the PS, the PVC pipe on the outside of the mortar specimen was used as a membrane, thereby simplifying the specimen sealing process. As shown in Figure 2(a), a rubber sleeve was tightened on the outside of the PVC pipe and the loading head. In the rubber sleeve, the tangential tension component which points to the axis of the specimen made the rubber sleeve tighten around the side of the PVC pipe and the loading head, so as to prevent the oil from penetrating into the end of the specimen.

To the TS, the heat-shrink sleeve, which was longer than the mortar specimen, acted as a membrane. It wrapped around the mortar specimen as well as both loading heads. Moreover, both ends of the heat-shrink sleeve were covered with the rubber sleeve, and the rubber sleeve was tightened around the heat-shrink sleeve and the loading head, as shown in Figure 2(b). When the multilayer heat-shrink sleeve is used, it is recommended that the outer heat-shrink sleeve should be longer and cover the both ends of the inner one.

Before wrapping the heat-shrink sleeve, we applied the quick-hardening cement to patch defects such as surface pores, to avoid the contact between oil and mortar caused by the rupture of the heat-shrink sleeve around the mortar surface. Although the mortar surface of PS cannot be patched, the PVC pipe does not break easily even if it is squeezed into holes under the action of oil, thanks to the PVC pipe's suitable ductility and thickness. In the present test, the phenomenon of oil leakage was not found in the mortar specimen sealed with the PVC pipe (PS).

2.4. Experimental Setup and Loading Procedure. The tests were conducted on an electrohydraulic servo-controlled triaxial testing machine (XTR01). The plunger of the confining cell is equipped with a self-balancing mechanism. The actual axial compressive stress of the specimen is σ_1 ($=p+q=p+F/A$), where p is the confinement applied by oil, q means the deviatoric stress applied by the plunger, F indicates the axial load measured by the load transducer, and A represents the cross-sectional area of the mortar specimen. Figure 3(a) illustrates the mechanical model of a mortar specimen. Axial and radial extensometers were used to measure the deformation of the specimen, as shown in Figure 3(b). Both ends of the axial extensometer were fixed on the loading heads, and the measured deformation

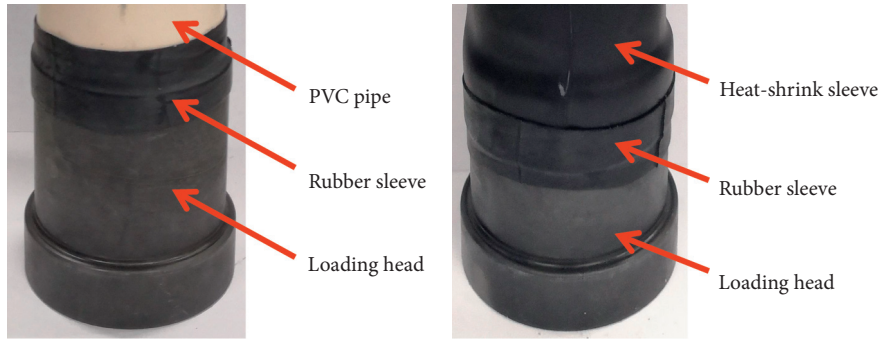

Figure 2: Sealing detail. (a) PS. (b) TS.

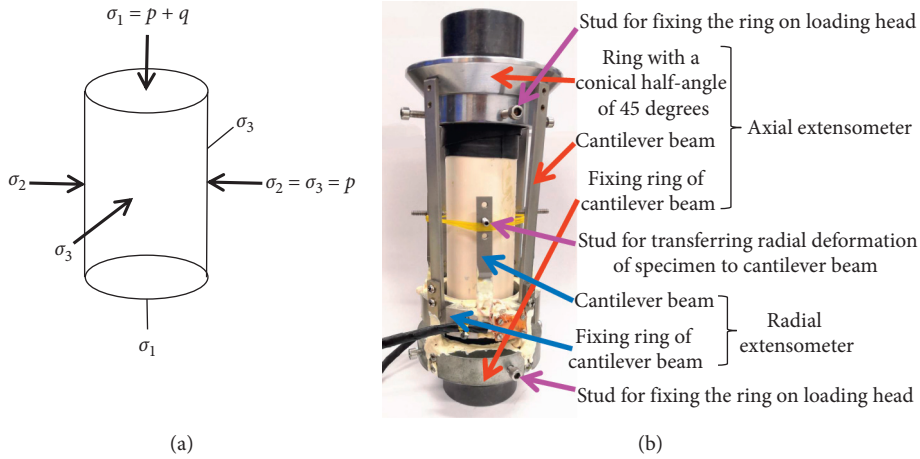

Figure 3: (a) Mechanical model of mortar. (b) Placement of extensometers.

covered two parts. One is the deformation of the entire specimen. The other is the deformation of the loading heads in the 45 mm height range. The deformation of the loading heads should be subtracted in data processing. The strains of two perpendicular directions in the middle of the specimen were measured using the radial extensometer. The dynamic and static strain apparatus continuously collected load and deformation data at the collecting frequency of 5 Hz.

The loading processes of PS and TS include the following six steps: (1) start collecting data and record zero points of axial load (F) and confinement (p); (2) the specimen is axially precompressed, and at the same time, the end face of the upper loading head is automatically in parallel contact with the end face of the plunger through the rotation of the spherical joint; (3) p is applied at a rate of 0.1–0.2 MPa/s until the designed value, and then p remains constant until the deformation tends to be stable. The viscoplastic deformations of both the mortar and the heat-shrink sleeve (or the PVC pipe) are released; (4) the axial displacement is applied at a constant rate of 0.002–0.004 mm/s; (5) after the deformation of the specimen reaches the critical value, the axial displacement at a rate of 0.01 mm/s is reduced until F is 0, and then p at a rate of 0.1–0.2 MPa/s is also reduced to 0; (6) the data collection is terminated.

The confinements of 0, 5, 10, 20, 40, and 70 MPa are selected for the tests. Each specimen corresponds to one of the confinements, and two specimens of the same type are tested under each confinement. It is required that under each confinement, the difference between the peak deviatoric stresses of two identical specimens is less than 7% of their average value. In case oil leakage or any other reason in the test distorts the experimental result, and so it is necessary to increase the number of the corresponding specimens.

2.5. Two Test Methods. We report two methods for conventional triaxial tests of mortar. The innovative method (so-called PMM) includes the following four steps: (i) the mortar is cast by using a PVC pipe as a mould. (ii) The mortar specimen is processed with the PVC pipe to meet the requirements for its size, shape, and precision. The specimen after processing is called PS. (iii) To seal the PS, the PVC pipe on the outside of the mortar specimen acts as a sealing membrane. (iv) The triaxial loading is performed on the specimen. It must be noted that, as a membrane with certain shear strength and shear stiffness, PVC pipe's influence on the mechanical behavior of mortar cannot be simply ignored and need to be studied.

The traditional test method (so-called TMM) also consists of the following four steps: (i) the mortar is cast by using a PVC pipe as a mould. (ii) The mortar specimen is processed with the PVC pipe to meet the requirements for its size, shape, and precision. Then the PVC pipe is removed, and the processed specimen is called TS. (iii) To seal the TS, the heat-shrink sleeve acts as a sealing membrane. (iv) The triaxial loading is performed on the specimen. It is worth noting that since the shear strength and the shear stiffness of the heat-shrink sleeve are very small, its influence on the mechanical behavior of mortar is negligible.

Our present work includes three kinds of mortar specimens, namely, the ultrahigh-strength mortar (UM) of 150 MPa, the high-strength mortar (HM) of 82 MPa, and the low-strength mortar (LM) of 17 MPa. To facilitate our discussion in the subsequent sections, we take P and T as a presymbol to represent PMM and TMM, respectively. For example, P-HM indicates a high-strength mortar specimen tested by PMM.

3. Mechanical Property Tests of PVC Pipes

3.1. Conventional Triaxial Compression Tests of PVC Pipes. In this work, we regard compressive for stress or strain as positive. ε_1 is the axial strain, ε_2 and ε_3 are the two perpendicular radial strains in the middle of the specimen, ε_r is the average value of radial strains, $\varepsilon_r = (\varepsilon_2 + \varepsilon_3)/2$.

The conventional triaxial tests for the PVC pipe with a height of 17 ± 0.5 mm were performed to understand its mechanical properties. To ensure that the oil pressure inside and outside the PVC pipe is equal, the PVC pipe's end face was designed to contain grooves with a depth of less than 0.4 mm and a width of less than 0.3 mm. q-ε_r and q-ε_1 curves of the PVC pipes are shown in Figure 4. As the confinement rises, the peak deviatoric stress of the PVC pipe increases slightly. The stress-strain curves of the PVC pipe on the whole coincide under different confinements before the peak point, which indicates that the impact of the confinement on deformation is practically negligible. After the peak point, the load decreases for PVC pipe's instability, and the radial and axial deformations increase rapidly. One can find from Figure 5 that the middle section of the damaged PVC pipe shows an obvious bulge. Additionally, the failure modes of PVC pipes are basically identical under other confinements.

The elastic modulus E is defined by the approximate straight line portion before the peak point. As indicated in Table 2, the elastic modulus of the PVC pipe is slightly enhanced at 5 MPa confinement, compared with zero confinement. However, under the confinements of 5–70 MPa, the elastic modulus of the PVC pipe does not change substantially.

3.2. Hydrostatic Pressure Tests of PVC Pipes. To further understand the deformation characteristics of PVC pipes under hydrostatic pressure, only the confinement was applied during the test. The confinement change with time (t) is given in Figure 6(a). It is found from Figure 6(b) that the radial compression deformation (D_r) gradually increases with the confinement enhancement. According to the geometric equation, all of the parameters, namely, the inner diameter, the outer diameter, and the thickness of the PVC pipe, decrease under hydrostatic pressure. When the confinement is stable, the variation range of the extensometer is less than 0.003 mm, which is far less than the radial deformation of the mortar specimen. Therefore, if the confinement remains constant, we can consider the thickness of the PVC pipe as an invariant factor.

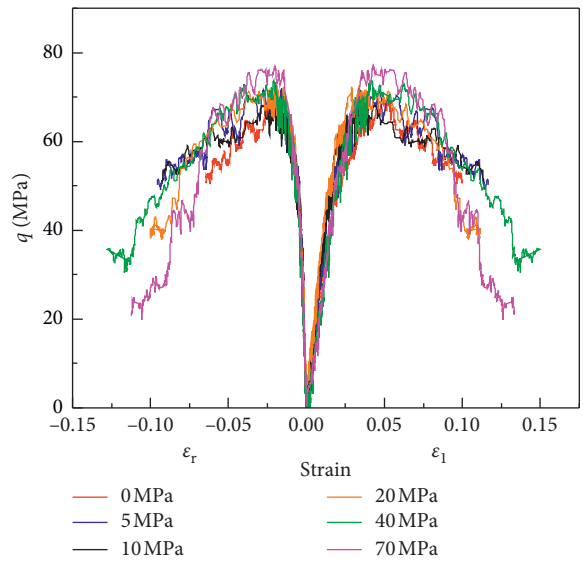

Figure 4: q-ε_r and q-ε_1 curves of the PVC pipes.

4. Conventional Triaxial Tests of Mortar

4.1. Failure Modes. By TMM, we can obtain the failure modes of specimens under different confinements, as shown in Figure 7. It is found that both the strength and the confinement influence the failure modes of mortar specimens. When the confinement is zero, splitting failures appear in T-UM and T-HM. Numerous vertical cracks are developed and divide the specimen into several crushed blocks. Shear failures occur both in T-UM under the confinements of 5–40 MPa and in T-HM under the confinements of 5–20 MPa. Additionally, a major inclined crack appears in these specimens. When T-UM is under the confinement of 70 MPa and T-HM is under the confinements of 40–70 MPa, they swell in a certain height range, with no strain localization.

In PMM, however, we can also present the failure modes of specimens under different confinements, as indicated in Figure 8. After the uniaxial compression in P-UM and P-HM, vertical and nearly vertical cracks which appear in both mortar specimens inside the PVC pipe (MIP) are significantly less than those of the same type specimens subjected to the uniaxial compression in TMM. After P-UM under the confinements of 5–40 MPa and P-HM under the confinement of 5 MPa, a diagonal shear band separately appears in the corresponding PVC pipe. Each MIP has a major inclined crack in the same position. Besides, the mortar blocks on both sides of the major inclined crack also

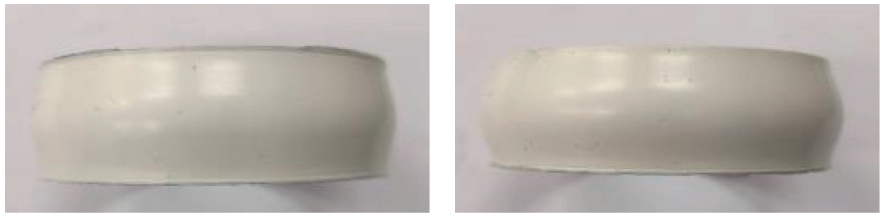

(a) (b)

Figure 5: Failure modes of the PVC pipes. (a) $p = 0$ MPa and (b) $p = 70$ MPa.

Table 2: Elastic modulus of the PVC pipes.

Confinement (MPa)	0	5	10	20	40	70
E (GPa)	2.5	3.0	3.0	2.9	2.7	2.9

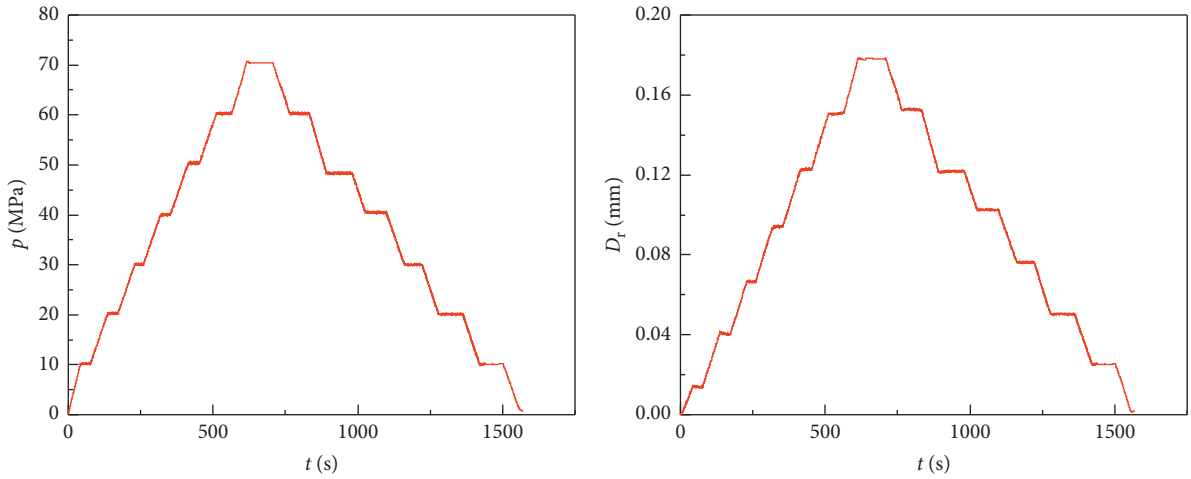

(a) (b)

Figure 6: The relationships between (a) p and t and (b) D_r and t.

show approximate transverse cracks, but none of them passes through the major inclined cracks. After the confinement of 70 MPa to P-UM and the confinements of 10–70 MPa to P-HM, it is several approximate transverse cracks rather than inclined cracks that appear in MIP.

The transverse cracks in MIP come as a result of interaction between the PVC pipe and MIP during loading and unloading. In the process of increasing confinement alone or only applying axial displacement under the constant confinement, both PVC pipe and MIP are axially compressed. Additionally, the MIP also yields axial compressive plastic deformation during the application of axial displacement. In the process of reducing the axial displacement to the load F approaching zero under the constant confinement, both PVC pipe and MIP are axially elongated, but no transverse crack is generated. This is because the confinement still exists. Even at the low confinement of 5 MPa, the axial load acting on the specimen due to the confinement is still close to 10 kN, so no transverse crack is formed. In the process of reducing the confinement to zero, the PVC pipe and MIP still undergo axial elongation. Since the elastic elongation and the deformability of the PVC pipe are greater than those of MIP, the transverse cracks in MIP are caused by tension.

One can find from Figure 9 that the end face of MIP is lower than that of the PVC pipe after triaxial loading. But, they are in the same plane before loading, which indicates that the rebound amount of the PVC pipe is larger than that of MIP. In Figure 8, after P-UM is subjected to triaxial loading under the confinements of 5–40 MPa, the approximate transverse cracks appearing in MIP do not pass through the major inclined crack, indicating that the transverse cracks are formed after the major inclined crack. It coincides with the explanation that the transverse cracks are generated during unloading. Also, the surfaces of the transverse cracks of MIP are relatively flat, and there is almost no powder generated by friction between the surfaces. These features are consistent with the characteristics of the tensile surfaces.

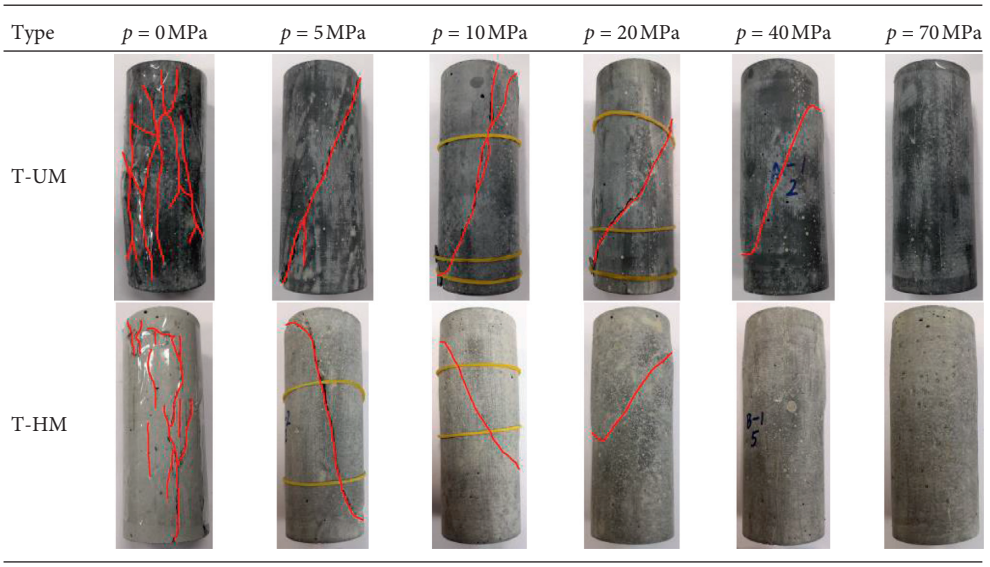

Figure 7: Failure modes of specimens tested by TMM under different confinements.

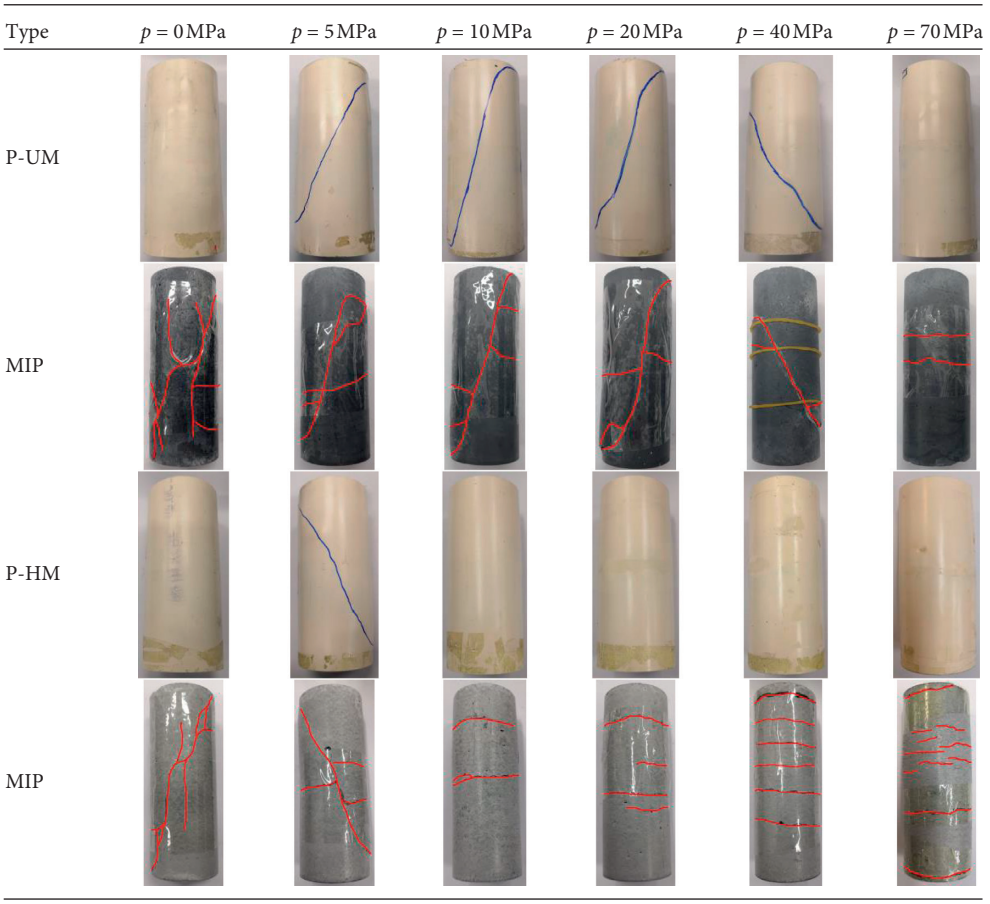

Figure 8: Failure modes of specimens tested by PMM under different confinements. *Notes*. MIP: mortar specimen inside the PVC pipe.

The axial compression of P-HM is relatively large under high confinements. After loading termination, MIP becomes a cylinder extruded from powder particles, and its tensile strength is almost zero. Therefore, in the process of reducing the confinement, the PVC pipe is more likely to crack MIP, leading to more transverse cracks. If the compression of P-UM is large enough, dense transverse cracks will develop in MIP.

Piotrowska et al. [23] found that four kinds of concrete containing coarse aggregates also formed multiple

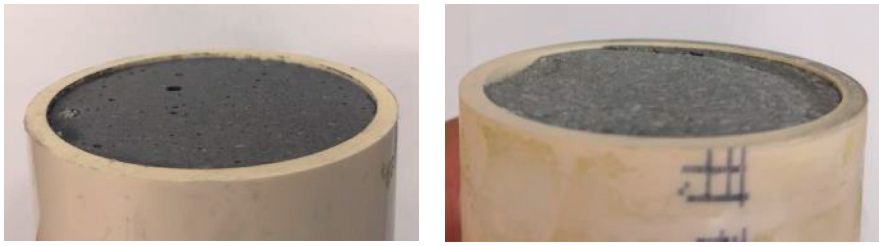

(a) (b)

Figure 9: End faces of specimens after triaxial loading. (a) P-UM. (b) P-HM.

transverse cracks after undergoing triaxial loading with 650 MPa confinement. Similar phenomena also occurred in the recycled aggregate concrete under high confinements after exposure to high temperatures [24]. It was pointed out in [23] that the transverse cracks were generated in the later stage of unloading, but the reason for this was not given. We hypothesize that the cause of the transverse cracks in [23] is the same as that in PMM, which is also the result of the tensile deformation of the membrane on the concrete during unloading. Since the membrane of the cylinder specimen ($\Phi 70 \times 140$ mm) in [23] is composed of 8 mm of latex and 2 mm of neoprene, the concrete has basically lost its cohesion in unloading, and the tension generated by the rebound of the membrane suffices to pull the concrete apart.

4.2. Stress-Strain Relationships. Figure 10 shows the q-ε_r and q-ε_1 curves of the mortar specimens through TMM and PMM. Some of the descendings are characterized by a straight line (as shown in Figure 10(a) with the confinements of 0, 5, 10, and 20 MPa, respectively), which are caused by the insufficient stiffness of the testing machine. The deformation corresponding to this straight line is completed instantly. Thus, only data at both ends of the straight line are collected. When the axial deformations of T-HM and P-HM increase to a certain extent under the confinements of 40 and 70 MPa, the stress-strain relationships tend to be flat, and then there seems to be no deterioration phenomenon. Xie et al. [25] experimentally found that when the confinement exceeds 50% of the uniaxial compressive strength of concrete, the stress does not drop after the peak point, which is similar to the above situation. Similar phenomena have been observed in rocks [26]. Zingg et al. [27] found that under very high confinement, the concrete behavior is influenced to a lesser extent by the matrix strength and is being essentially governed by the granular stacking of the concrete. Nevertheless, it is worth noting that this conclusion is only valid for dry concrete, and the presence of water in capillary porosity will certainly modify concrete behavior, especially for concrete with low matrix strength under very high confinement [28, 29].

4.3. Radial Interaction between PVC Pipe and MIP under Uniaxial Compression. Table 3 shows the uniaxial compressive strength of three strength mortar specimens by PMM and TMM. As expected, the uniaxial strength obtained by PMM is higher than that by TMM. The explanations for this are as follows.

In PMM, the PVC pipe can improve the mortar strength not only by applying radial pressure to MIP, but also by bearing the axial load. As can be seen from Table 2, the elastic modulus of the PVC pipe is 2.5 GPa, about 7% of UM. Additionally, the cross-sectional area of the PVC pipe is less than 25% of the MIP cross-sectional area. In uniaxial compression tests, the axial load borne by the PVC pipe at the peak point is about 1.5% of MIP in P-UM, 2.6% of MIP in P-HM, and 8.8% of MIP in P-LM. We, therefore, conclude that the axial load borne by the PVC pipe can be ignored.

Under uniaxial compression, the q-ε_1 and u_r-ε_1 relationships between the mortar specimens with three strengths and the PVC pipe are plotted in Figure 11. Here, we regard the expansion as negative. In one case, u_r indicates the deformation along the diameter direction for the mortar specimen. In the other case, u_r is the deformation along the inner diameter direction for the PVC pipe. We assume that the PVC pipe is just in contact with the surface of MIP before the axial strain (ε_1) is applied, but the radial pressure is zero. At the beginning of loading, u_r of the PVC pipe is larger than that of the mortar. As ε_1 increases further, u_r of the mortar increases rapidly. When reaching a stress level before the peak point, the u_r-ε_1 curve of the mortar intersects the u_r-ε_1 one of the PVC pipe, and ε_1 at the intersection is recorded as ε_{1c}. After that, u_r of the mortar is larger than that of the PVC pipe. For PMM, in the process of applying ε_1 on the specimen, when $0 < \varepsilon_1 < \varepsilon_{1c}$, the PVC pipe is separated from MIP, and the radial pressure between them approaches zero. When $\varepsilon_1 > \varepsilon_{1c}$, the PVC pipe starts to contact with MIP and then exerts radial pressure on MIP. As can be seen from Figure 11, ε_{1c} of three mortar specimens is smaller than the respective axial strain at the peak point. This means that MIP is subjected to the radial pressure exerted by the PVC pipe before the peak point, so the uniaxial strength obtained by PMM is higher than that by TMM (as also referred in Table 3).

4.4. Strength Characteristics. We define the peak stress (σ_{max}) of the mortar specimen as $q_{max} + p$, where q_{max} is the peak deviatoric stress and p is the confinement. An average of σ_{max} of the same two types of specimens under the identical confinement is denoted as $\overline{\sigma}_{max}$. The $\overline{\sigma}_{max} - p$ curves drawn from the experimental data by two methods are shown in Figure 12, in which abundant information can

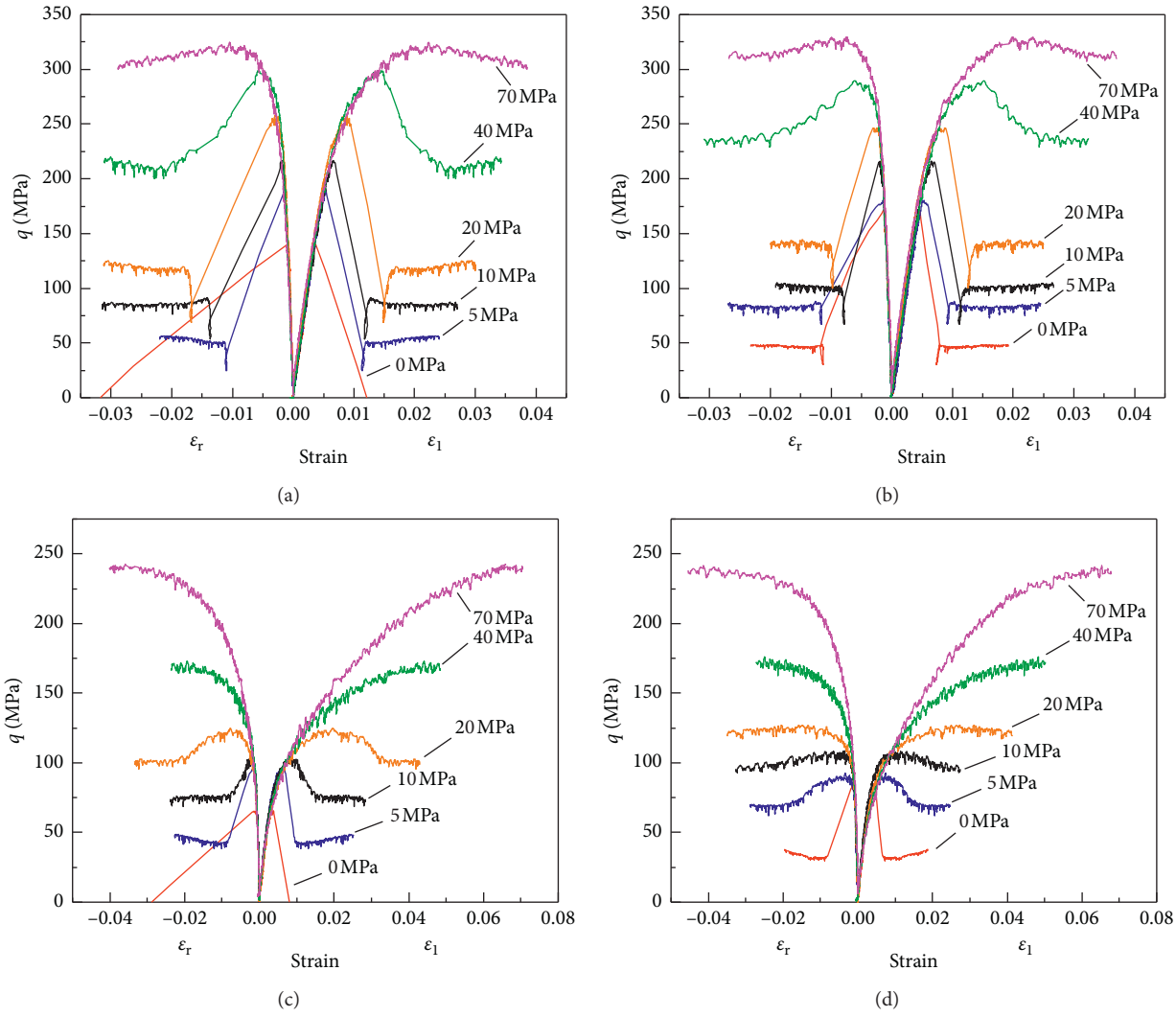

Figure 10: q-ε_r and q-ε_1 curves of mortar specimens. (a) T-UM. (b) P-UM. (c) T-HM. (d) P-HM.

Table 3: Uniaxial compressive strengths of mortar specimens with three strengths (MPa).

Type	Strength
T-UM	143.0
T-HM	70.0
T-LM	14.1
P-UM	168.0
P-HM	85.0
P-LM	20.3
P-UM-end friction reduction	164.5
P-HM-end friction reduction	84.0

Notes. The friction-reducing pad consists of three layers of polytetrafluoroethylene (PTFE) with a thickness of 0.1 mm.

be employed to analyze the mechanical properties of the mortar.

When the confinement ranges from 5 to 70 MPa, the $\overline{\sigma}_{max} - p$ curve of P-UM coincides with the corresponding one of T-UM, and P-HM against T-HM has similar characteristics as well. We naturally conclude that there is a

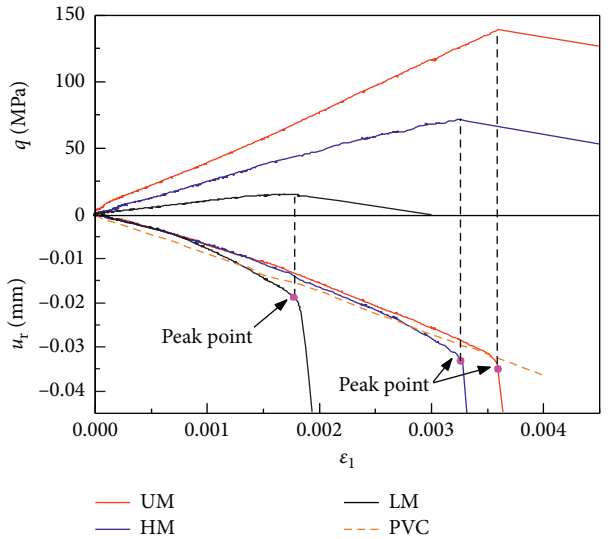

Figure 11: q-ε_1 and u_r-ε_1 relationships between the mortar specimens with three strengths and the PVC pipe.

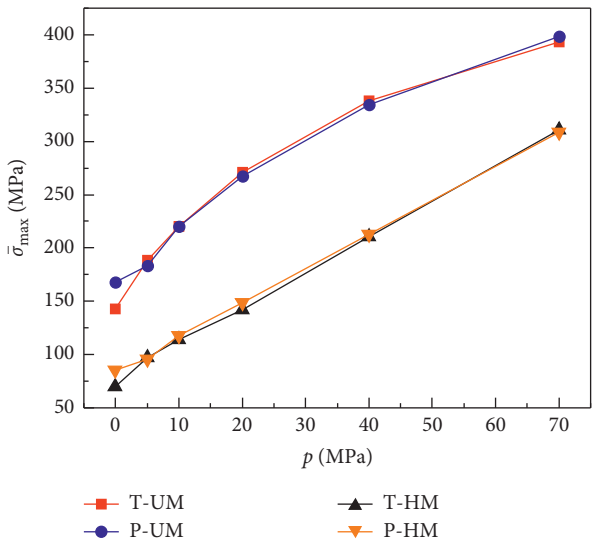

Figure 12: $\overline{\sigma}_{max} - p$ curves of mortar.

characteristic confinement p_0. When $p < p_0$, the strength obtained by PMM is greater than that by TMM, whereas when $p > p_0$, the strengths by these two methods are almost identical. For the PVC pipes and the mortar used here, $0 < p_0 \leq 5$ MPa. Additionally, PMM can replace TMM to obtain the triaxial strength of mortar when $p > p_0$.

For T-UM, when $0 \leq p \leq 70$ MPa, the relationship between $\overline{\sigma}_{max}$ and p is a monotonically rising upward convex curve. With the increase in p, the slope of the curve gradually decreases and finally approaches a constant. To T-HM, when 5 MPa $< p \leq 70$ MPa, $\overline{\sigma}_{max}$ has a linear relationship with p. When $0 \leq p \leq 5$ MPa, the $\overline{\sigma}_{max} - p$ curve has data only at both ends. Based on the characteristics of the mortar material, the missing data between both ends should be described by a nonlinear curve. Comparing the $\overline{\sigma}_{max} - p$ curves of mortar with two different strengths, we conclude that there should be a strong correlation between the mortar strength and the nonlinear relationship of $\overline{\sigma}_{max}$ versus p. The higher the mortar strength, the larger the confinement range corresponding to the nonlinear curve.

For UM, HM, and LM, the difference in uniaxial strengths obtained by PMM and TMM is 25.0, 15.0, and 6.2 MPa, respectively. Such strength difference is associated with the mortar strength. The higher the mortar strength, the greater the strength difference. As can be seen from Figure 12, when the confinement approaches zero, the slope of the $\overline{\sigma}_{max} - p$ curve of P-UM is larger than that of P-HM. If a confinement increment starts from zero, such increment should have a more significant influence on the compressive strength for P-UM than that for P-HM. As the MIP expands radially, the confining effect of the PVC pipe on MIP is equivalent to the confinement.

It can be seen from Table 3 that the end friction has little influence on the mortar strength when PMM is employed, which is inconsistent with the generally accepted viewpoint. The reason is that the confinement weakens the influence of the tensile stress caused by the friction-reducing layer on the mortar strength [30], and the confining effect of the PVC pipe on the mortar is similar to the confinement, which can also weaken the effect of the friction-reducing layer.

4.5. Residual Strength. In Table 4, the residual strengths by PMM are significantly higher than those by TMM at zero confinement or lower confinements, whereas there is basically no difference at higher confinements. Taking UM as an example, this phenomenon can be explained from the perspective of failure modes:

(1) $p = 0$.

The damaged T-UM forms several crushed blocks and almost has no residual strength, while the P-UM has a great residual strength. The residual strength arises from the radial pressure between the PVC pipe and the cracked MIP. When the relative displacement occurs between the crushed blocks, this generates not only the friction (f_1) between the crushed blocks, but also the friction (f_2) between surfaces of the crushed blocks and the inner wall of the PVC pipe. These two kinds of frictions jointly contribute to the residual strength of MIP of P-UM. Although the axial load borne by the PVC pipe under zero confinement can also enhance the residual strength, this enhancement is limited.

f_2 is closely associated with not only the radial pressure and the friction coefficient between the MIP and the PVC pipe, but also the shear stiffness and shear strength of the PVC pipe. f_2 can be ignored since the shear stiffness and shear strength of a heat-shrink sleeve are almost zero. On the contrary, f_2 must be taken into account because the PVC pipe has some shear stiffness and shear strength.

(2) $p = 5$–40 MPa.

Whether it is P-UM or T-UM, the damaged mortar is divided into two blocks by the major inclined crack. The residual strength of T-UM only depends on f_1, but the residual strength of MIP of P-UM is determined by f_1 and f_2. Therefore, even if the axial load directly shared by the PVC pipe is not taken into account, the residual strength by PMM should also be higher than that by TMM.

(3) $p = 70$ MPa.

Regardless of whether PMM or TMM is used for the triaxial test of UM, the damaged mortar shows no inclined crack. There is no f_2 since there is no discontinuous displacement inside the mortar during the application of the axial displacement. If the axial load shared by the PVC pipe is neglected, the residual strength of P-UM and T-UM should be approximately equal in theory.

4.6. Strain at the Peak Point. Figure 13 shows the relationships of confinement p versus ε_{1m} (axial strain at the peak point) and ε_{rm} (radial strain at the peak point), respectively. Since the confinement hinders the generation and expansion of mortar cracks, the deformability of mortar is

Table 4: Residual strengths of mortar specimens (MPa).

p (MPa)	T-UM		P-UM		Residual strength difference	T-HM		P-HM		Residual strength difference
	Residual strength	Failure mode	Residual strength	Failure mode		Residual strength	Failure mode	Residual strength	Failure mode	
0	0	SPF	48	SPF	48	0	SPF	35	SPF	35
5	55	SHF	83	SHF	28	44	SHF	68	SHF	24
10	82	SHF	103	SHF	21	73	SHF	95	SQF	22
20	120	SHF	142	SHF	22	98	SHF	123	SQF	25
40	211	SHF	235	SHF	24	165	SQF	170	SQF	5
70	305	SQF	310	SQF	5	240	SQF	238	SQF	−2

Notes. Splitting failure, shear failure, and squeeze flow are, respectively, expressed as SPF, SHF, and SQF.

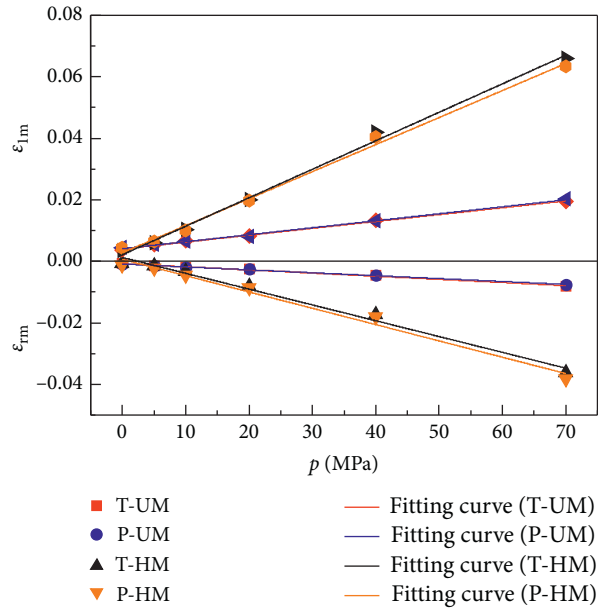

Figure 13: ε_{1m}-p and ε_{rm}-p curves of mortar.

improved. As the confinement increases, strain at the peak point of mortar increases linearly. A similar phenomenon occurs in concrete with different strengths and steel fiber-reinforced concrete [14, 15, 31, 32]. Under different confinements, strain at the peak point by PMM does not differ greatly from that by TMM.

4.7. Failure Criterion. Our test results show that the Mohr–Coulomb criterion can be used to describe the failure characteristics of mortar. This criterion is expressed as

$$\frac{\sigma_{max}}{f_c} = 1 + \frac{k\sigma_3}{f_c}, \tag{1}$$

where σ_{max} is the triaxial compressive strength ($\sigma_{max} = q_{max} + p$), f_c is the uniaxial compressive strength, σ_3 is the confinement ($\sigma_3 = p$), and k is a parameter of the Mohr–Coulomb criterion, related to materials. The value of k ranges from 2.6 to 5.3 for mortar with diversified strengths [32, 33], and our fitting results are also within this range.

As can be seen from Table 5, the fitting results of the Mohr–Coulomb criterion are in good agreement with the experimental data of HM. However, for T-UM, the relative coefficient R^2 is only 0.772 16, and the fitting results are not ideal. Newman [34] proposed the following equation to reflect the nonlinear relationship between confinement and strength:

$$\sqrt{A\left(\frac{\sigma_3}{f_c}\right)^2 + B\left(\frac{\sigma_3}{f_c}\right) + 1} - \frac{\sigma_{max}}{f_c} = 0, \tag{2}$$

where A and B are the Newman criterion parameters and other parameters are the same as those in equation (1).

Table 6 shows the fitting results of the Newman criterion, in which R^2 is higher than 0.99, indicating that the Newman criterion accurately predicts mortar failure. It can be found from Figure 14(a) that the Mohr–Coulomb criterion is suitable for describing the change trend of compressive strength of HM with confinement. However, it can only roughly reflect the change trend of compressive strength of

Table 5: Fitting results by using the Mohr–Coulomb criterion.

Type	k	R^2
T-UM	4.109	0.772 16
P-UM	3.612	0.934 36
T-HM	3.483	0.993 65
P-HM	3.192	0.999 15

Table 6: Fitting results by using the Newman criterion.

Type	A	B	R^2
T-UM	−14.921	20.667	0.999 85
P-UM	−3.876	12.865	0.991 82
T-HM	9.449	9.036	0.997 62
P-HM	10.467	6.207	0.999 19

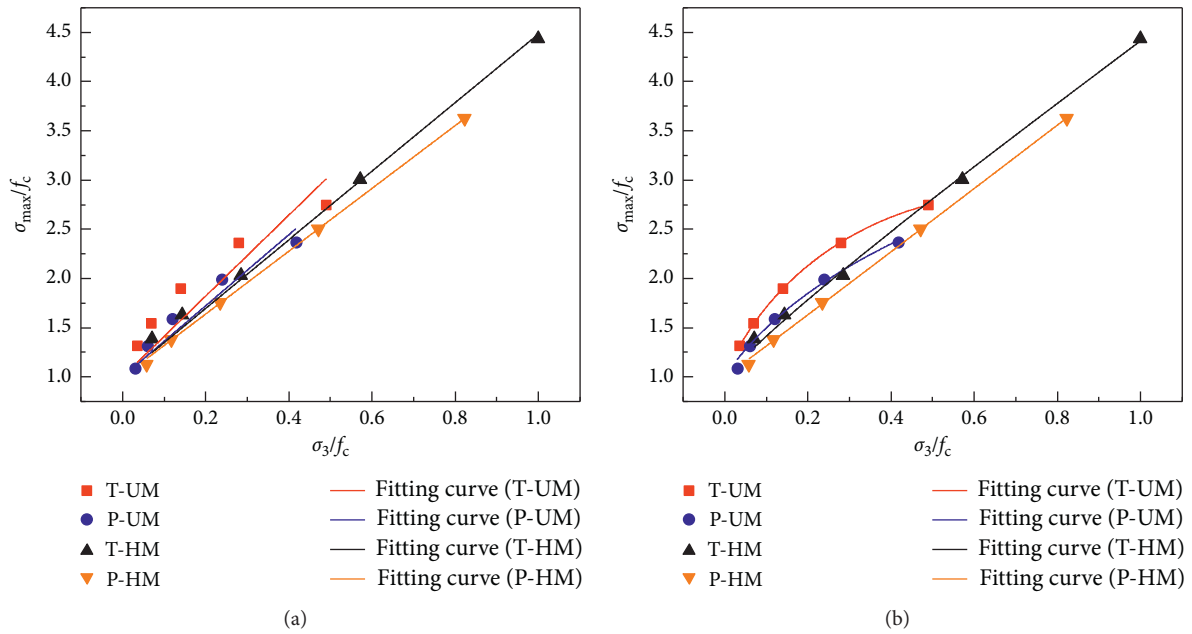

Figure 14: Comparison between fitting results and experimental data. (a) Mohr–Coulomb criterion. (b) Newman criterion.

UM. Figure 14(b) shows that the Newman criterion is more widely applicable to mortar with different strengths than the Mohr–Coulomb criterion.

5. Conclusions

We have performed a series of conventional triaxial tests on UM (82 MPa) and HM (150 MPa) by using PMM and TMM, respectively. Based on the test results, the following conclusions can be drawn:

(1) Compared with TMM, PMM has the advantages of avoiding cleaning, assembling, and disassembling the mould, facilitating the specimen processing, and simplifying the specimen sealing before the triaxial test. PMM, therefore, greatly improves the test efficiency.

(2) When the uniaxial compression test is conducted by PMM, the radial expansion of the inner wall of the PVC pipe is larger than that of MIP at the beginning of loading. When reaching a certain stress level before the peak point, the PVC pipe starts to contact with MIP which leads to the radial pressure between them. With appearance of the radial pressure, the uniaxial strength obtained by PMM is higher than that by TMM.

(3) In triaxial compression tests, there is a characteristic confinement p_0. When the confinement is higher than p_0, the strengths tested by PMM and TMM are almost identical. For the PVC pipes and the mortar used in the present work, the range of p_0 is 0–5 MPa.

(4) For UM and HM, when the confinement ranges are 0–40 MPa and 0–20 MPa, respectively, the residual strength by PMM is higher than that by TMM.

When the confinement ranges are 70 MPa and 40–70 MPa, respectively, the residual strengths by both methods are approximately identical. These behaviors are closely associated with the failure modes of mortar.

(5) When PMM is used for the test, the transverse cracks appearing in MIP after enduring a triaxial loading are the result of interaction between the PVC pipe and MIP.

Data Availability

The data used to support this study are available within the article.

Conflicts of Interest

The authors declare that there are no conflicts of interest regarding the publication of this paper.

Acknowledgments

This research was supported by the National Natural Science Foundation of China (nos. 51279003 and 51078024) and the National Key R&D Program of China (no. 2016YFC0600901).

References

[1] A. Gholampour, T. Ozbakkaloglu, and R. Hassanli, "Behavior of rubberized concrete under active confinement," *Construction and Building Materials*, vol. 138, pp. 372–382, 2017.

[2] I. Imran and S. J. Pantazopoulou, "Experimental study of plain concrete under triaxial stress," *ACI Materials Journal*, vol. 93, no. 6, pp. 589–601, 1996.

[3] S. Sinaie, A. Heidarpour, X. L. Zhao, and J. G. Sanjayan, "Effect of size on the response of cylindrical concrete samples under cyclic loading," *Construction and Building Materials*, vol. 84, pp. 399–408, 2015.

[4] H. Beshr, A. A. Almusallam, and M. Maslehuddin, "Effect of coarse aggregate quality on the mechanical properties of high strength concrete," *Construction and Building Materials*, vol. 17, no. 2, pp. 97–103, 2003.

[5] M. D. Ingraham, K. A. Issen, and D. J. Holcomb, "Response of castlegate sandstone to true triaxial states of stress," *Journal of Geophysical Research: Solid Earth*, vol. 118, no. 2, pp. 536–552, 2013.

[6] X. H. Vu, Y. Malecot, and L. Daudeville, "Strain measurements on porous concrete samples for triaxial compression and extension tests under very high confinement," *The Journal of Strain Analysis for Engineering Design*, vol. 44, no. 8, pp. 633–657, 2009.

[7] A. Cividini, A. Taliercio, G. S. Landriani, R. Bellotti, G. Ferrara, and P. Rossi, "An apparatus for cyclic tests on cylindrical concrete specimens," *Materials and Structures*, vol. 25, no. 8, pp. 490–498, 1992.

[8] Z. L. Wang, H. H. Zhu, J. G. Wang, and B. Zhu, "Experimental study on macroscopic mechanical behavior of SFRC under triaxial compression," *Mechanics of Advanced Materials and Structures*, vol. 19, no. 8, pp. 653–662, 2012.

[9] Y. Malecot, L. Daudeville, F. Dupray, C. Poinard, and E. Buzaud, "Strength and damage of concrete under high triaxial loading," *European Journal of Environmental and Civil Engineering*, vol. 14, no. 6-7, pp. 777–803, 2010.

[10] Z. Chen, Y. Hu, Q. Li, M. Sun, P. Lu, and T. Liu, "Behavior of concrete in water subjected to dynamic triaxial compression," *Journal of Engineering Mechanics*, vol. 136, no. 3, pp. 379–389, 2010.

[11] L. Bjerkeli, J. J. Jensen, and R. Lenschow, "Strain development and static compressive strength of concrete exposed to water pressure loading," *ACI Structural Journal*, vol. 90, no. 3, pp. 310–315, 1993.

[12] Q. Li and F. Ansari, "Mechanics of damage and constitutive relationships for high-strength concrete in triaxial compression," *Journal of Engineering Mechanics*, vol. 125, no. 1, pp. 1–10, 1999.

[13] R. Sovják, F. Vogel, and B. Beckmann, "Triaxial compressive strength of ultra high performance concrete," *Acta Polytechnica*, vol. 53, no. 6, pp. 901–905, 2013.

[14] D. C. Candappa, J. G. Sanjayan, and S. Setunge, "Complete triaxial stress-strain curves of high-strength concrete," *Journal of Materials in Civil Engineering*, vol. 13, no. 3, pp. 209–215, 2001.

[15] X. Lu and C.-T. T. Hsu, "Behavior of high strength concrete with and without steel fiber reinforcement in triaxial compression," *Cement and Concrete Research*, vol. 36, no. 9, pp. 1679–1685, 2006.

[16] D. A. Mishra and I. Janeček, "Laboratory triaxial testing—from historical outlooks to technical aspects," *Procedia Engineering*, vol. 191, pp. 342–351, 2017.

[17] T. Gabet, Y. Malécot, and L. Daudeville, "Triaxial behaviour of concrete under high stresses: influence of the loading path on compaction and limit states," *Cement and Concrete Research*, vol. 38, no. 3, pp. 403–412, 2008.

[18] G. Akovali, "Plastic materials: polyvinyl chloride (PVC)," *Toxicity of Building Materials*, vol. 5, no. 3, pp. 23–53, 2012.

[19] L. M. Alves and P. A. F. Martins, "Cold expansion and reduction of thin-walled PVC tubes using a die," *Journal of Materials Processing Technology*, vol. 209, no. 9, pp. 4229–4236, 2009.

[20] C. E. Kurt, "Concrete filled structural plastic columns," *Journal of the Structural Division*, vol. 104, no. 1, pp. 55–63, 1978.

[21] J.-Y. Wang and Q.-B. Yang, "Investigation on compressive behaviors of thermoplastic pipe confined concrete," *Construction and Building Materials*, vol. 35, pp. 578–585, 2012.

[22] A. S. Saadoon, "Experimental and theoretical investigation of pvc-concrete composite columns," University of Basrah, Basra, Iraq, Doctoral Dissertation, 2002.

[23] E. Piotrowska, Y. Malecot, and Y. Ke, "Experimental investigation of the effect of coarse aggregate shape and composition on concrete triaxial behavior," *Mechanics of Materials*, vol. 79, pp. 45–57, 2014.

[24] E. Meng, Y. Yu, J. Yuan, K. Qiao, and Y. Su, "Triaxial compressive strength experiment study of recycled aggregate concrete after high temperatures," *Construction and Building Materials*, vol. 155, pp. 542–549, 2017.

[25] J. Xie, A. E. Elwi, and J. G. Macgregor, "Mechanical properties of three high-strength concretes containing silica fume," *ACI Materials Journal*, vol. 92, no. 2, pp. 135–143, 1995.

[26] S.-Q. Yang, Y. Ju, F. Gao, and Y.-L. Gui, "Strength, deformability and X-ray micro-CT observations of deeply buried marble under different confining pressures," *Rock Mechanics and Rock Engineering*, vol. 49, no. 11, pp. 4227–4244, 2016.

[27] L. Zingg, M. Briffaut, J. Baroth, and Y. Malecot, "Influence of cement matrix porosity on the triaxial behaviour of concrete," *Cement and Concrete Research*, vol. 80, pp. 52–59, 2016.

[28] Y. Malecot, L. Zingg, M. Briffaut, and J. Baroth, "Influence of free water on concrete triaxial behavior: the effect of porosity," *Cement and Concrete Research*, vol. 120, pp. 207–216, 2019.

[29] X.-D. Vu, M. Briffaut, Y. Malecot, L. Daudeville, and B. Ciree, "Influence of the saturation ratio on concrete behavior under triaxial compressive loading," *Science and Technology of Nuclear Installations*, vol. 2015, Article ID 976387, 10 pages, 2015.

[30] Z. Wang and L. C. Wu, "Triaxial test study of reactive powder concrete with different sizes under different friction reducing conditions," *Journal of Zhejiang University (Engineering Science)*, vol. 53, no. 1, pp. 40–50, 2019, in Chinese.

[31] F. Ansari and Q. B. Li, "High-strength concrete subjected to triaxial compression," *ACI Materials Joumal*, vol. 95, no. 6, pp. 747–755, 1998.

[32] G. M. Ren, H. Wu, Q. Fang, J. Z. Liu, and Z. M. Gong, "Triaxial compressive behavior of UHPCC and applications in the projectile impact analyses," *Construction and Building Materials*, vol. 113, pp. 1–14, 2016.

[33] Y. Farnam, M. Moosavi, M. Shekarchi, S. K. Babanajad, and A. Bagherzadeh, "Behaviour of slurry infiltrated fibre concrete (SIFCON) under triaxial compression," *Cement and Concrete Research*, vol. 40, no. 11, pp. 1571–1581, 2010.

[34] J. B. Newman, "Concrete under complex stress," *Development in Concrete Technology*, vol. 1, pp. 151–219, 1979.